Q. J. R. Meteorol. Soc. (1998), **124**, pp. 793–809

A thermal oscillation under a restorative forcing

By WENJU CAI[1]* and PETER C. CHU[2]
[1]*CSIRO, Australia*
[2]*Naval Postgraduate School, Monterey, USA*

(Received 12 July 1996; revised 14 June 1997)

SUMMARY

The authors report an interdecadal oscillation in a wind- and thermally-driven ocean general circulation model (OGCM). The oscillation is tantalizing in that it occurs under a relatively strong thermal damping (26.3 $W m^{-2}K^{-1}$). Examinations involving a two-dimensional OGCM, a simple thermal 'flip–flop' model, and a three-dimensional OGCM with and without the nonlinear effect of temperature in the state equation of sea water demonstrate that the oscillation is not driven by mechanisms such as the so-called convective oscillator, or the advective overshooting oscillator. Instead, the oscillation is associated with the propagation of modelled long Rossby-waves with westward phase velocity. It is found that the north–south basin extent of the OGCM is an important factor; a larger north–south basin extent is conducive to the generation of thermal wind flows crucial for initiating the propagation of disturbances. The geophysical relevance of these results is discussed.

KEYWORDS: Interdecadal oscillations Restorative forcing Rossby waves Thermal circulation

1. INTRODUCTION

Interdecadal variabilities have been studied extensively in ocean general circulation models (OGCMs). Oscillations induced by saline forcing (e.g. Marotzke 1990; Weaver and Sarachik 1991a,b; Wright and Stocker 1991; Winton and Sarachik 1993; Huang 1994; Huang and Chou 1994; Cai 1995; Chen and Ghil 1995) are usually examined in models under so-called mixed boundary-conditions (that is, the use of a restoring boundary-condition on surface temperature and a flux boundary-condition on surface salinity (Bryan 1986)). Oscillations induced by thermal forcing (e.g. Cai *et al.* 1995; Greatbatch and Zhang 1995; Cai 1996) have been examined in a purely thermal, or thermally-dominant, system. Most of these studies explain the oscillation as driven by an advective overshooting oscillator. In a thermal system, the argument goes as follows. When the overturning is stronger than the average, heat storage increases at high latitudes. This reduces the contrast between densities at pole and equator, and weakens the overturning circulation, which, in turn, reduces the poleward heat-transport and leads to a high-latitude cooling. The pole to equator density contrast then increases, accelerating the overturning, and the process repeats itself.

Lenderink and Haarsma (1994) and Pierce *et al.* (1995) considered the competing roles of thermal and saline forcing components in determining the stability of a water column. Both studies emphasized the role of a convective oscillator. Lenderink and Haarsma (1994) found that, depending upon the comparative role of the two forcing components, the water column could have three different regimes: one permanently convective, one permanently non-convective, and one oscillatory (periodically switching between the convective and non-convective regimes). Pierce *et al.* (1995) proposed another kind of convective oscillator. They showed that, in order for oscillations to occur in their model, the nonlinear effect of temperature in the state equation of sea water is a necessary condition. The mechanism is supported by an analytical, two-layered 'flip–flop' model.

Recently, the role of the coastal wave-guide has been emphasized. This is associated with the thermohaline adjustment in the generation of oceanic variability (Greatbatch and

* Corresponding author: CSIRO, Division of Atmospheric Research, PMB1 Aspendale, Victoria 3195, Australia.

Peterson 1996; Winton 1996). The adjustment problem was first studied by Davey (1983) and further explored by Wajsowicz and Gill (1986). In a spin-down of an OGCM driven by a density field that varies only in the meridional direction, Wajsowicz and Gill (1986) found the importance of viscous, baroclinic boundary-waves in the model adjustment process. The problem has also been addressed by Winton (1996). He extended the early studies to include the the propagation of boundary waves in regions of formation of weakly- or non-stratified deep-water in models driven by a constant heat-flux forcing alone. He found that under a constant heat-flux forcing, generation of interdecal oscillation was a robust feature. It involves periodic growth and decay of a baroclinic disturbance, which propagates cyclonically around the basin. The result is confirmed by Greatbatch and Peterson (1996) in an OGCM, again under a constant heat-flux forcing. These authors believed that the waves in their studies were Kelvin waves, although strictly speaking Kelvin waves were not resolved in their models because of the low resolution.

Griffies and Tziperman (1995) interpreted the oscillation in the Geophysical Fluid Dynamics Laboratory (GFDL) coupled atmosphere–ocean model (Delworth *et al.* 1993) as an external excitation of a damped oscillatory thermohaline mode by the stochastic effects of the atmospheric variability. This is in sharp contrast to the explanation given by Cai *et al.* (1995) and Greatbatch and Zhang (1995), who concluded that the oscillation might be an internal oceanic process. In their ocean-only models, driven by a constant heat-flux forcing, they were able to produce many oscillation features similar to those observed in the North Atlantic (Deser and Blackmon 1993; Kushnir 1994), and to those of the interdecadal oscillations in the GFDL coupled model (Delworth *et al.* 1993). Latif and Barnett (1994, 1996) focused on interdecadal climate variability over the North Pacific Ocean and North America. They found that the modes involve unstable ocean–atmosphere interactions over the North Pacific, and that the time scale of the oscillation is mainly determined by that of baroclinic planetary waves, which are generated by anomalies in wind-stress curl.

In this study, we report an interdecadal oscillation under a restorative forcing in an OGCM similar to that reported by Cai *et al.* (1995). The tantalizing aspect of the oscillation is that it occurs under a relatively strong thermal damping (26.3 W $m^{-2}K^{-1}$). This result is in sharp contrast to those found in previous studies (e.g. Cai *et al.* 1995; Greatbatch and Peterson 1996; Winton 1996). In these studies, a flux condition was required for persistent oscillations and the possibility of oscillations under a restorative forcing was not examined.

As can be seen from the above discussion, there are a number of possible mechanisms for oscillations. Which of the above, if any, is responsible for the generation of the oscillation in the present study? An important clue is that oscillations are easily induced in the present model but were not so in the work reported by Cai *et al.* (1995). We begin our exploration by describing the difference in model configurations between the present study and that of Cai *et al.* (1995) in section 2. In section 3, we show the generation of the oscillation under a relatively strong thermal damping rate, and the low dependence upon initial conditions. In section 4, possible causes are examined. We show that the oscillation in our study is not driven by a convective oscillator, nor by an advective overshooting oscillator. In section 5, we demonstrate that the oscillation is associated with boundary-wave propagation, and that the wave is a long Rossby-wave (with westward phase velocity), rather than a Kelvin wave as in the studies of Winton (1996) and Greatbatch and Peterson (1996). We show that basin length is an important factor for the generation of the oscillation. A larger north–south extent of the ocean basin enables this mechanism to operate so effectively that it can sustain a considerable damping, and that a flux condition is not required. The implication and the geophysical relevances of the oscillation are discussed in section 6.

TABLE 1. DISTRIBUTION OF VERTICAL LEVELS

Level	Thickness (m)	Depth of (T, S) (m)
1	25.0	12.5
2	25.0	37.5
3	40.0	70.0
4	70.0	125.0
5	110.0	215.0
6	200.0	370.0
7	330.0	635.0
8	450.0	1025.0
9	650.0	1575.0
10	900.0	2350.0
11	900.0	3250.0
12	900.0	4150.0

TABLE 2. STANDARD VALUES OF MODEL COEFFICIENTS

Parameter	Symbol	Value ($m^2\ s^{-1}$)
Horizontal diffusivity	A_{TH}	1×10^3
Horizontal viscosity	A_{MH}	3×10^5
Vertical diffusivity	A_{TV}	1×10^{-4}
Vertical viscosity	A_{MV}	1×10^{-4}

2. THE MODEL

This study employs the version of the Bryan–Cox–Semtner OGCM used by Pacanowski *et al.* (1991), which is based on the work of Bryan (1969). The state equation is that described by Gill (1982), and includes the full nonlinear effect of temperature. In all experiments, there is no salinity forcing and the salinity is kept constant and uniform. The horizontal grid spacing is 4° of latitude by 4° of longitude. The model has twelve levels in the vertical, at depths listed in Table 1. Values assigned to the various model parameters are listed in Table 2. These are the same as those used by Cai (1995), Cai and Godfrey (1995) and Cai *et al.* (1995). The model domain is a flat-bottomed, two-hemisphere Atlantic basin. It has a width of 60° and, in the basic cases, a length of 144° extending from 72°S to 72°N. This extends the model used by Cai *et al.* (1995) in the north–south direction by one model grid-point in each hemisphere. In some cases the basin length is shortened or extended for testing the sensitivity to basin length. The southern hemisphere includes a modelled Antarctic Circumpolar Current (ACC) passage from 48°S to 64°S, and a sill 2350 m deep in the model's Drake Passage. Cyclic conditions are applied there. This sill is intended to provide a realistic ACC transport by setting up a bottom pressure difference between the two sides of the passage south of Cape Horn (Gill and Bryan 1971; Holland 1973; Cai 1994). Otherwise, the flat bottom would lead to an unrealistically large wind-driven ACC; so one has to specify an ACC (see Cai and Godfrey 1995). Another small modification from the model used by Cai *et al.* (1995) is the inclusion of a model Weddell Sea to allow an Antarctic Circumpolar Convective cell. (Detailed layout can be seen in Fig. 7.)

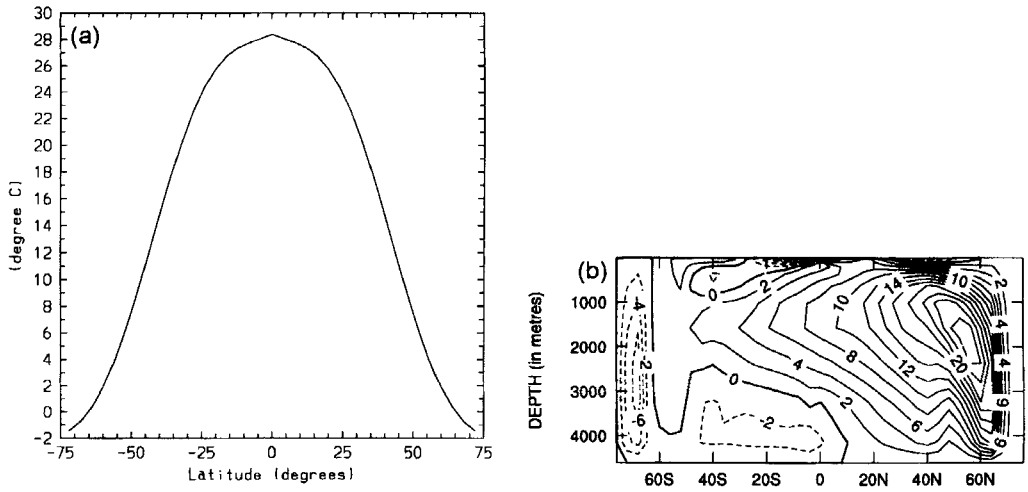

Figure 1. (a) Surface relaxation temperature (°C), and (b) overturning stream function (Sv) for R15o, that is, under a restoration with a restoring time of 15 days, and initiated from a resting ocean.

TABLE 3. DETAILS OF MODEL EXPERIMENTS DISCUSSED IN SECTION 3

Run	Initial Condition	Model Domain	Forcing	Persistent Oscillations
R15o	Rest	72°S to 72°N	Restoring (15 d)	none
R45	R15o	72°S to 72°N	Restoring (45 d)	24.7 y
R45o	Rest	72°S to 72°N	Restoring (45 d)	23.7 y
R30o	Rest	72°S to 72°N	Restoring (30 d)	none
R45oShtB	Rest	64°S to 64°N	Restoring (45 d)	none
2DR45o	Rest	72°S to 72°N	Restoring (45 d)	none
LnrR45o	Rest	72°S to 72°N	Restoring (45 d)	24.6 y
R45of0	Rest	72°S to 72°N	Restoring (45 d)	none
R45ShtBp	R45oShtB	64°S to 64°N	Restoring (45 d)	none
R30p	R30o	72°S to 72°N	Restoring (30 d)	none
R45o0.5ω	Rest	72°S to 72°N	Restoring (45 d)	16.8 y
R45o1.5ω	Rest	72°S to 72°N	Restoring (45 d)	37.2 y

The fifth column indicates whether or not persistent oscillations occurred. If yes, the period is given in years (y).

3. INITIAL MODEL RESULTS

(*a*) *Model spin-up*

Initially, the OGCM was spun up by restoring the temperature at the uppermost level to a zonally uniform value given by the profile shown in Fig. 1(a), which approximates the observed zonally averaged field. This run is referred to as R15o (see Table 3), and starts from a resting ocean (denoted by 'o'). The profile has the analytical expression used by Cai *et al.* (1995) and the expression applies to the extended model domain from 68° to 72°. The restoring time is 15 days (hence the '15' in R15o). This corresponds to a thermal coupling strength of 79 W $m^{-2}K^{-1}$. The model is also subject to the wind stress used by Bryan (1987). The wind stress is symmetric about the equator, and mimics well the observed wind stress with features of strong westerlies at mid-to-high latitudes and moderate easterlies in the tropics. In all model runs, the wind is kept constant. The

lower-level acceleration techniques of Bryan (1984) are not used at any stage. After about 4000 years of integration, the spin-up reaches a statistically steady state. The overturning circulation is shown in Fig. 1(b), and is qualitatively similar to that in the real Atlantic Ocean. It features a northern sinking cell, an ACC convective cell, and a northern intrusion cell from the south. The model ACC reaches 104 Sv. The modelled circulation is of the conveyor-belt type and is similar to that described by Cai *et al.* (1995).

(*b*) *Oscillation under a restorative condition*

Initiated from the steady state of R15o, R45 (Table 3) was carried out, in which the temperature at the uppermost level was relaxed to the same climatology (Fig. 1(a)) but with a restoring time of 45 days. At the moment of changing the surface forcing, the surface heat-flux was suddenly and uniformly reduced to one third of that before the change. The reduction of the heat flux shocked the system somewhat initially but, as it recovered, oscillations with a period of 24.7 years appeared. These can be seen in Fig. 2(a), which shows the time series of the overturning sampled at a location (60°N, 2350 m) near the place where the overturning of the steady state of R15o is a maximum. Unless otherwise stated, all single-point time-series of overturning were taken at this location.

Since R45 was initiated from the steady state of R15o, a question arises as to what would happen if the OGCM were spun up from the same steady state as R15o, that is a resting ocean. To this end, R45o (Table 3) was carried out. Figure 2(b) shows the time series of the overturning. Oscillations persist. The period is 23.7 years. Thus the oscillation is almost independent of the initial condition. In fact, from Fig. 2(b) we see that the oscillation occurred at the early stage of the spin-up and initially had large amplitudes. The amplitudes reduced as the integration proceeded until a stage was reached when they stablized. The reduction was due to the weakening (damping) effect associated with the restoring forcing. This can be further illustrated from a time series (Fig. 3(a)) for run R30o (Table 3). This run was identical to R45o, except that the restoring time was 30 days. Initially the evolution of the overturning resembled that of R45o but the oscillation was eventually damped.

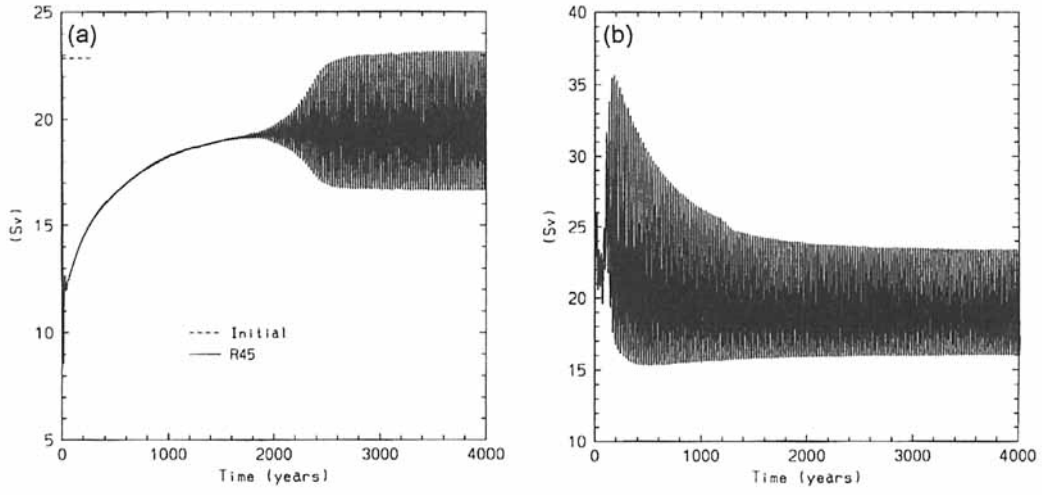

Figure 2. (a) Time series of the overturning (Sv) for run R45, that is, initiated from the steady state of R15o and under a restoration with a restoring time of 45 days. The overturning is sampled at a location (60°N, 2350 m) near the place where the overturning of the steady state of R15o is a maximum. (b) Time series of the overturning (Sv) for run R45o, that is, under a restoration with a restoring time of 45 days but initiated from a resting ocean.

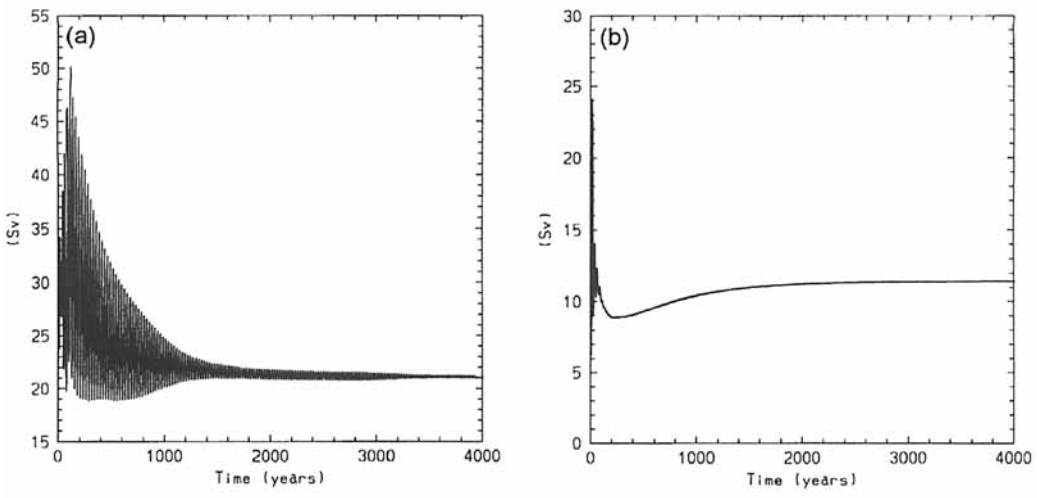

Figure 3. (a) Time series of the overturning (Sv) for R30o, that is under a restoration with a restoring time of 30 days and initiated from a resting ocean. (b) Time series of the overturning for run R45oShtB, that is in a model with a short north–south basin extent, under a restoration with a restoring time of 45 days, and initiated from a resting ocean.

The oscillation is interesting, especially when compared with the result of Cai *et al.* (1995) who found that, even under a diagnosed heat-flux forcing (without the damping effect from the surface restoration) no oscillation occurred. A heat-flux redistribution was necessary for the generation of oscillations. As commented upon earlier, the only difference between the present model and that of Cai *et al.* (1995) is that the north–south extent of the model basin is 4° (one grid-length) longer in the present model in each hemisphere. The extent of model basin appears to be important. To test this, run R45oShtB (Table 3) was carried out. This run was identical to R45o except that the basin extent was from 64°S to 64°N, two grid-lengths shorter than that in the R45o case. This is chosen to facilitate a clear-cut comparison between the short basin (R45oShtB) and the long basin (R45o) cases. Since the restoring temperature took the same profile as in R45o (Fig. 1(a)), the restoring temperature at the polar boundary in this run was warmer than that in R45o. Figure 3(b) shows the evolution of the overturning. We see that no persistent oscillation was produced. Note that the maximum overturning in the northern hemisphere in R45oShtB is of a comparable size to that in R45o, but moves southward, so that the overturning shown is smaller.

4. Some possible causes of the oscillation

Consider run R45o and R45oShtB. One may ask several questions. Is it the lower restoring temperature at the polar boundary, or the associated change in wind, that is important as a result of the north–south extension of the basin? Or is it that the exact latitude is important? Or is it rather that a large initial extent of the convective region predisposes the model towards increased variability, since convection is intermittent even at the spin-up equilibrium? In order to answer these questions, many experiments have been carried out using both the long- and short-basin configurations of the model. The results indicate that it is the extent of the basin, rather than changes in the restoring temperature

or the wind stress, which accounts for the different behaviour of the circulation between the short- and long-basin cases.

A significant contrast in the evolution of the overturning between long-basin cases (e.g. R45o) and short-basin cases (e.g. R45oShtB) is that the oscillations develop in the initial stage (e.g. the first 500 years) in the former but are absent from the early stage of integration in the latter. This suggests that, from the initial stage, the adjustment process in the long- and short-basin cases is quite different.

In what follows, we show that the oscillation in our study is not driven by a convective oscillator, nor by an advective overshooting oscillator. Since we are dealing with a thermal system, the convective oscillator proposed by Lenderink and Haarsma (1994) does not operate here. Work by Pierce *et al.* (1995) using a 'flip–flop' model *implicitly* suggested that, when density is a nonlinear function of temperature, oscillations may be induced, even in a purely thermal circulation. In all the experiments described so far, the nonlinear effect of temperature in the state equation is included. In order to test if this oscillator is responsible for the oscillation in our OGCM, an analysis was carried out using a simplified thermal-only version of the two-layered flip–flop model. Details are given in an appendix. The simplified flip–flop model allowed a surface cooling and the associated heat loss. In order to maintain a heat budget, the lost heat was re-introduced into the system as a subsurface heating. As shown in the appendix, because of the nonlinear effect of the temperature in the state equation, such a thermal system may, depending on the magnitude of the subsurface heating, have three different regimes: one permanently convective, one permanently non-convective, and one oscillatory (periodically switching between the convective and non-convective regimes).

There are at least two ways to check if the mechanism works in our OGCM. Firstly, the flip–flop model suggests that once the nonlinear effect of temperature in the state equation is removed, no oscillation occurs. However, when R45o was repeated with a density equation set to that in the flip–flop model, giving run LnrR45o (Table 3), oscillations still occurred. This indicates that the nonlinearity is not what drives the oscillation in our OGCM. Additional support can be found from the work of Huang and Chou (1994) who used a salinity-driven model, in which persistent oscillations were produced despite the state equation's being nearly linear in salinity. Secondly, if the mechanism in the flip–flop model is what drives the oscillations in our OGCM, then oscillations should also occur in a two-dimensional version of the OGCM. To test this inference, we carried out run 2dR45o (Table 3). The east–west extent was reduced to two model tracer-grids (that is, only one velocity grid) and there were no east or west boundaries. Other details were identical to R45o. No persistent oscillation resulted, further confirming that the convective oscillator displayed in the flip–flop model was not the cause of the oscillation in our OGCM. Indeed, an examination shows that the subsurface heating obtained from the OGCM near the polar regions was generally greater than that required for oscillations to occur in the flip–flop model. The no-oscillation solution in 2dR45o also suggests that the advective-overshooting oscillator is not what drives the oscillation in our OGCM either.

5. Oscillation and wave propagation

A detailed examination reveals that the oscillation in the present study is associated with waves that propagate along the model northern boundary. The wave propagation for run R45 can be seen in Fig. 4. It shows the evolution of the rates of change of heat content HC, which is defined as

$$\mathrm{HC} = \int_{-h}^{0} c_p \rho_0 T \, \mathrm{d}z.$$

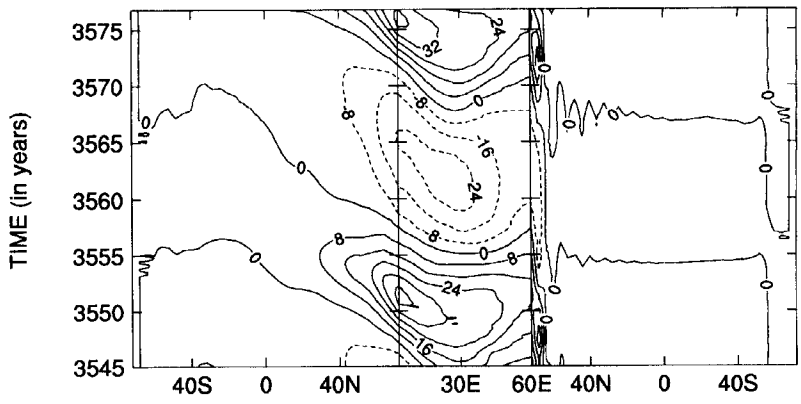

Figure 4. Evolution of the rates of change of heat content over water columns along water grids nearest to the western, northern and eastern boundaries. The distance is measured clockwise from the south-western end of the model domain and is plotted as a straight line. The contour interval is 8 W m^{-2}.

Here c_p is the specific heat capacity and ρ_0 is the reference density. Rates of change in heat content are therefore described by $\partial HC/\partial t$. Shown in Fig. 4, is this quantity over water columns at grid points nearest to the western, northern, and eastern land boundaries. The distance along the boundaries is measured clockwise from the south-western end of the model domain and is plotted as a straight line. The plot covers a period from year 3545 to year 3577 (see Fig. 2(a)). Several features emerge. Firstly, most of the time of an oscillation is spent in propagation along the weakly or non-stratified boundary, that is along the northern boundary. Along this boundary, the propagation speed is slow and the amplitude large. By contrast, along stratified boundaries the propagation speed is much faster and the amplitude much smaller. Secondly, anomalies propagate faster during increasing heat-content than during decreasing heat-content. Finally, an oscillation period is the sum of the time for positive and negative anomalies to cross the basin.

To reveal the interrelationship between the wave properties and the thermohaline circulation, the evolution of the overturning covering the same period is shown in Fig. 5(a), and the anomalies of overturning and sea-surface temperature (SST) from a mean circulation every quarter period are shown in Figs. 6 and 7 respectively. The overturning reaches a maximum at year 3550 and a minimum at year 3560. A quarter period before the overturning reaches the maximum, the northern boundary is occupied by cool anomalies (as can be inferred from Fig. 7(d)). This means that, at that time, the anomaly of the north–south pressure gradient is largest. From then until the time of maximum overturning, the meridional northward flow increases (Fig. 6(d)) and this is associated with an increase in the east–west pressure gradient and the development of a positive SST anomaly in the east (Fig. 7(d)) on the way. The anomalous northward flow not only pumps a heat anomaly into the north-eastern corner, but also causes the anomaly to propagate westwards (Fig. 4). The weak or non-existent stratification along the northern boundary impedes the movement along the leading edge, allowing more heat to be accumulated at the front, leading to the increase in amplitude. Then, from year 3550 to year 3554, the heat content increases. At year 3552 and near the north-western corner, it increases at the greatest rate. An animation clearly shows that the wave front turns southward in this corner. It then propagates along the western boundary with increasing speed and reducing amplitude. During this time, the northern boundary is occupied by positive SST anomalies (Fig. 7(a, b)). The large heat increase in the north-western corner then leads to a decrease in the east–west pressure

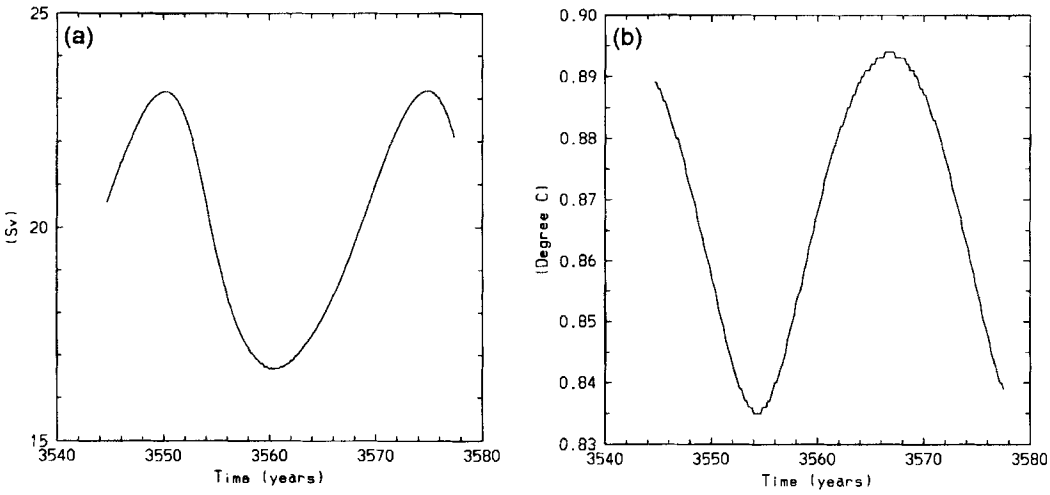

Figure 5. (a) Time series of the overturning for R45 covering a 33-year period starting from year 3545. The overturning reaches a maximum at year 3550 and a minimum at year 3560. (b) Time series of the temperature averaged over the northern half of the northern-hemisphere model basin, subtracted from the temperature over the southern half of the northern-hemisphere model basin. The maximum of the associated density-gradient leads the maximum of the overturning by about 6 years, that is by about 90°.

gradient and in the overturning (Fig. 6(a, b)). From year 3554 to year 3560, the overturning decreases from below the mean (Fig. 6(b, d)) to a minimum, and cold anomalies develop at the north-eastern corner and propagate westwards, associated with the opposite phase of the oscillation.

The feature of wave propagation can also be seen in the phase relationship between the strength of the overturning circulation and the north–south density difference. Figure 5(b) shows the difference between temperatures averaged over the northern and southern halves of the northern-hemisphere model basin. Comparing panels (a) and (b) of Fig. 5, we see that the maximum in the density gradient leads the maximum overturning by about 6 years, that is by about 90°.

The above features are somewhat similar to those found by Winton (1996) and Greatbatch and Peterson (1996). However, the wave in these two studies was a Kelvin wave. In order to identify the nature of the wave in the present study, R45of0 was carried out. This experiment was identical to R45o except that, north of 22°N, β-effects were switched off, and a constant Coriolis parameter (that for 22°N) was used. No oscillation was generated. The generation of Kelvin waves does not require the presence of β-effects. The lack of wave generation when β-effects were absent suggests that the wave in the present study was not a Kelvin wave. Instead it was a long Rossby wave with westward phase velocity. In the absence of any bottom topography, such long Rossby waves, may be generated in the presence of β-effects. This is so in our OGCM.

The Rossby wave in the present study was forced by density anomalies in the north-eastern corner of the basin. This being so, the speed of anomalies across the basin was determined by the slowly varying forcing and did not need to match that of a free Rossby wave. However, in order to gain an impression of the relationship between the oscillation period and the phase velocity of the model Rossby waves, we approximate the phase velocity of the modelled waves by that of a free Rossby wave. For a free Rossby wave, the phase velocity may be expressed in terms of $\beta c^2 / f_0^2$, where c is the stratified gravity

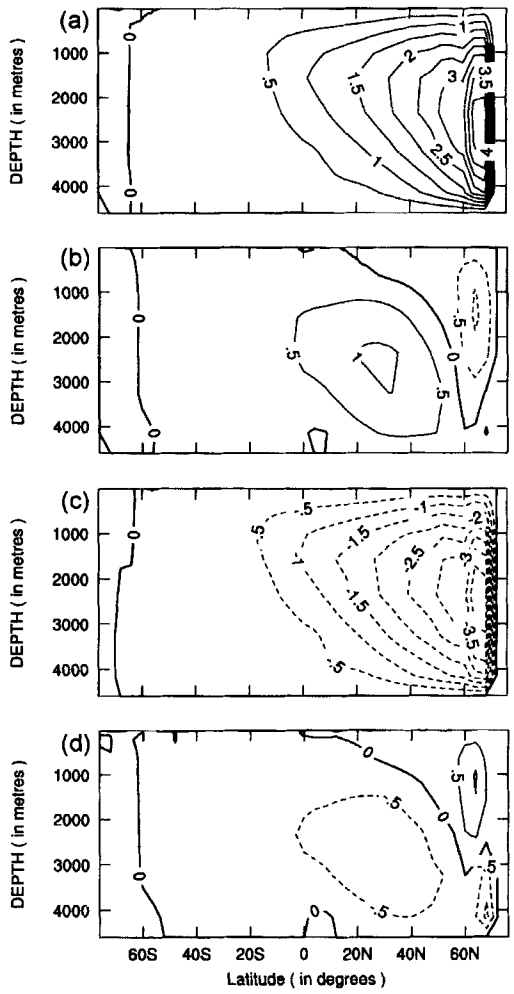

Figure 6. Anomalies of overturning (Sv) from a mean circulation for R45 at about a quarter period interval: (a) at year 3550; (b) at year 3554; (c) at year 3560; (d) at year 3569. Panels (a) and (d) show the anomalies when the overturning is at a maximum and a minimum respectively.

wave speed and f_0 is the Coriolis parameter (Gill 1982). Since anomalies propagate faster during increasing heat-content than during decreasing heat-content, and since an oscillation period is the sum of the time for positive and negative anomalies to cross the basin, we obtained from R15 two vertical profiles of zonal-mean density of the northern-most grids, one averaged over the period of increasing heat content and one over the period of decreasing heat-content. The two profiles were then used to calculate the stratified gravity-wave speed during increasing (c_I) and decreasing (c_D) heat-content. We then employed the method for decomposition of vertical modes detailed by Gill (1982) and boundary conditions applicable to the rigid lid and a flat ocean-bottom (Moore and Philander 1977). The two profiles give the first mode c_I and c_D of 0.441 and 0.392 m s^{-1}, corresponding to times needed to travel from east to west along the northern boundary, using a latitude ϕ of 70°, of 9.03 and 11.44 years, respectively. The total time is therefore 20.7 years, close to the oscillation period.

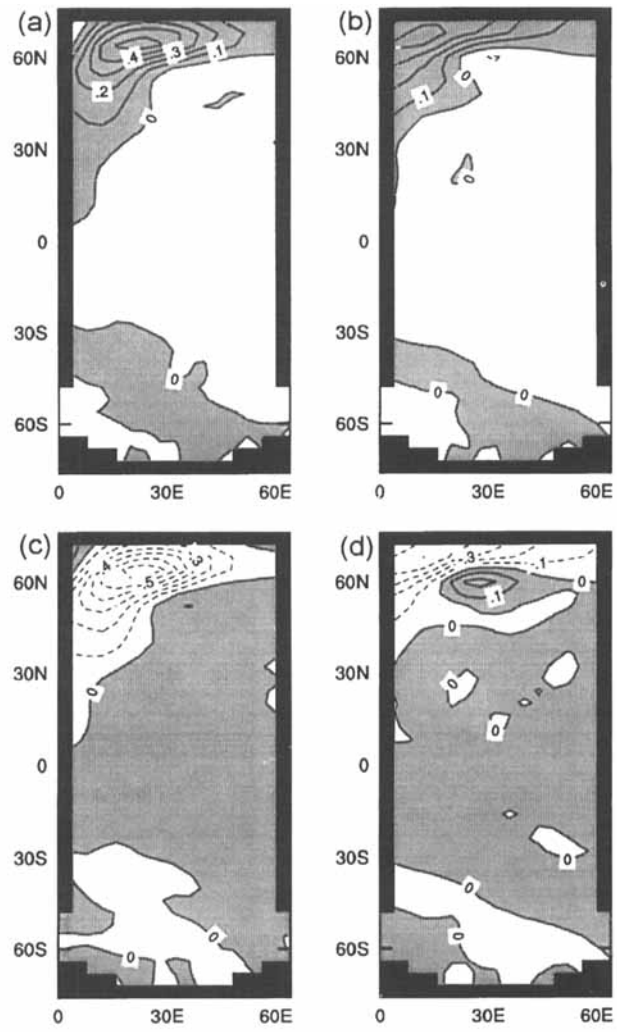

Figure 7. As Fig. 6, but for SST anomalies.

The oscillation mechanism is clearly quite sensitive to the presence of β effects. In order to ensure that the zero-beta change in run R450f0 did not have influences beyond suppressing the Rossby waves and to further confirm the Rossby-wave mechanism, we have run two more experiments, in which the rotation speed of the earth ω is changed by a factor of 0.5 (decrease) and 1.5 (increase). These two experiments are referred to as R45o0.5ω and R45o1.5ω, respectively. Other details of the experiments are identical to those of R45o. The oscillation periods for R45o0.5ω and R45o1.5ω are 16.8 years and 37.2 years. Note that, as ω changes, both β and f_0 change. Using the approximation of a free Rossby wave, the phase velocity may be rewritten as $c^2 \cos\phi/2R\omega \sin^2\phi$, where R is the radius of the earth. Thus, as ω decreases (increases), the phase velocity increases (decreases) and the oscillation period becomes shorter (longer), consistent with the model result. The dependence on ω is not linear, because some changes in c take place. These experiments therefore lend support to the Rossby mechanism.

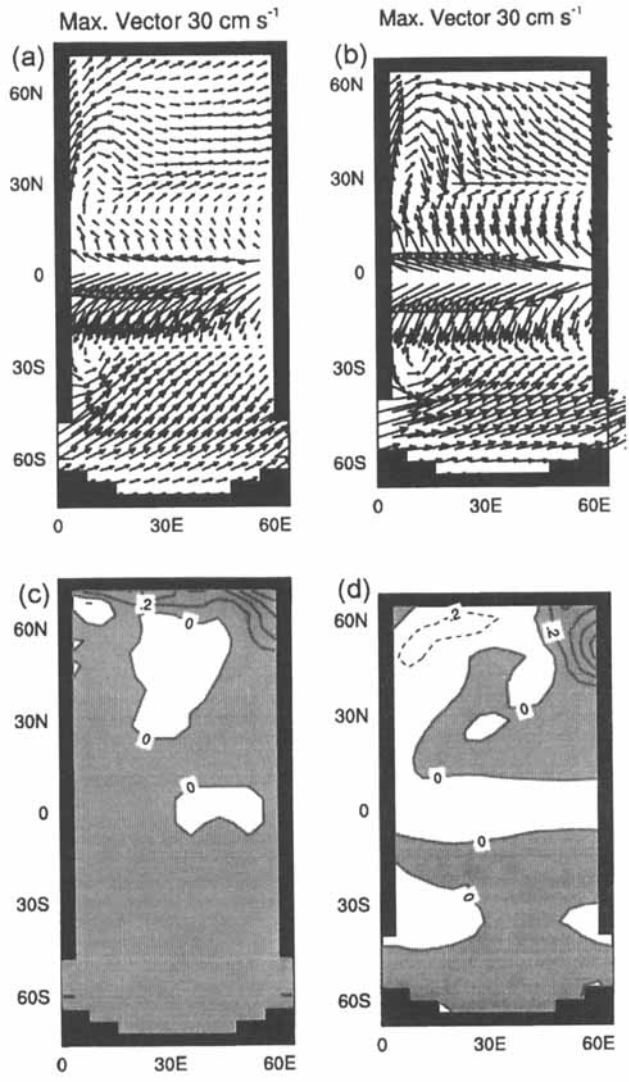

Figure 8. (a) and (b) Steady surface flow vectors of R30o and R45oShtB respectively. From the steady state of these two runs, runs R30p and R45ShtBp are initiated. In each run a heat anomaly is imposed over the three northern-most grid-points along the eastern boundary, and lasts for six months; (c) and (d) distribution of SST anomaly (°C) 5 years after the anomaly is removed for R30p and R45ShtBp respectively.

Why is the basin extent important for the generation of the oscillation? In cases with a larger north–south extent, maximum overturning is allowed to take place at a higher latitude, and convection is more concentrated in the north-eastern corner. This favours the generation of thermal wind currents normal to the weakly stratified northern boundary. This can be seen from the steady surface-flow of R30o and R45oShtB shown in Figs. 8(a, b). The flows of these two runs are different. In R30o, in the region near the north-eastern corner and along the northern boundary, there are considerable northward flow components. By contrast, in R45oShtB, there are considerable southward components. The northward flows in R30o are important in flushing the anomaly in the north-eastern corner so that it propagates along the northern boundary. (Recall that the adjustment process

in these two runs is completely different.) This difference in the flows accounts for the different adjustment processes in the long- and short-basin cases. In R30o, the favourable flow condition leads to a significant role of the long-Rossby-wave propagation at the early stage of the integration. This is why strong oscillations take place (Fig. 3(a)), although they gradually weaken and are eventually damped by the restoring forcing. By contrast, in R45oShtB, oscillations are absent from the early stage of the integration (Fig. 3(b)).

To confirm this point further, two more experiments were carried out, designated R30p and R45ShtBp (Table 3) respectively. They started from the steady state of R30o and R45oShtB, but each with a heat-flux anomaly imposed for six months in the three northernmost grid-points of the eastern boundary. At the end of six months, the heat-flux anomaly was removed instantaneously, and the SST anomaly in the north-eastern corner in each case was about 5°C. Figure 8(c, d) shows the anomaly distribution five years after the anomaly was removed for R30p and R450ShtBp respectively. We see that only in R30p does the anomaly propagate along the northern boundary.

It should be stated that the sensitivity to the model north–south basin extent may vary with model resolution and viscosity. For reasons of numerical stability, low-resolution OGCMs usually require the use of a large viscosity. It is reasonable to suspect that different resolution and viscosity may lead to different conclusions with regard to the effects of basin extent. Greatbatch and Peterson (1996) have shown that, in their model under a flux forcing, a smaller viscosity leads to oscillations which are otherwise absent. In order to test the sensitivity to viscosity, we have carried out two runs identical to R45oShtB and R45o except that a horizontal viscosity one-third of that in these two runs was used. The results show that, even with the smaller viscosity, no oscillation is produced in the short-basin case while in the long-basin case persistent oscillations occur. Examination reveals that the difference in flow structure between the short- and long-basin cases discussed above are seen in these two new experiments.

6. Discussion and Conclusions

We describe an interdecadal oscillation in a wind- and thermally-driven OGCM under a restorative forcing. Examinations involving a two-dimensional OGCM, a simple thermal 'flip–flop' model, and a three-dimensional OGCM with or without the nonlinear effect of temperature in the state equation demonstrate that the oscillation is not driven by mechanisms apparent in the so-called convective oscillator, or the advective overshooting oscillator. Instead, the oscillation occurs in association with the generation of long Rossby waves propagating westwards. Phase velocities predicted by theoretical work (Gill 1982) give a time for a wave to travel from east to west along the northern boundary that is approximately the same as the oscillation period.

That oceanic Rossby-waves play a role in the generation of decadal oscillations has already been reported by other authors. Latif and Barnett (1994, 1996) described decadal modes over the North Pacific Ocean and North America in a coupled ocean–atmosphere model. In their model, oceanic Rossby-waves and their effects on the large-scale oceanic circulation largely determined the anomaly patterns associated with the decadal modes. The Rossby waves in their model were driven by wind-stress changes. The present results show that Rossby waves can be generated by density changes and play a significant role in the generation of decadal and interdecadal oscillations.

One of the most interesting features of the present study is that the oscillation occurs under a relatively strong restoring boundary condition. Winton (1996) found that a constant heat-flux forcing is required for persistent oscillations. Under a constant heat-flux forcing, the zonally integrated circulation of an OGCM is constrained by the (implied constant)

oceanic heat transport. The constraint is quite strong, and the imposed heat-loss at high latitudes must be carried out even when the model convection adjustment is switched off. Locally, the forced circulation is constrained by a constant rate of heat divergence or convergence. Cai (1995) has discussed the consequences when these constraints cannot be accommodated by the model internal circulation. The main finding in his study is that the system will oscillate persistently. The anomaly associated with the oscillation develops and decays periodically, there being no damping from air–sea thermal interactions. In the present model, such constraints were not applied, so that the rate of convergence or divergence was allowed to change. Winton (1996) reported a case under a restoring forcing with a restoring timescale ten times that used in the spin-up (equivalent to a restoring time of 250 days over a 25 m mixed layer), and with a reference buoyancy-range increased by a factor of four. Initial oscillations were seen but none persisted. In our model, under a 30-day restoration, oscillations were damped, but a timescale longer than this produced persistent oscillations. We have shown that a long north–south basin extent is conducive to the generation of meridional flows normal to the weakly or non-stratified boundary. These flows are crucial for the generation of persistent oscillations. In view of these results, it seems that the sensitivity to damping timescale may depend upon many model parameters, and probably strongly upon the flow conditions near the polar boundary.

The implication of an oscillation under a constant heat-flux forcing is that oceanic variabilities may be an internal process, rather than forced externally as suggested by Griffies and Tziperman (1995). Such an implication can be transferred to the present study because, firstly, the restoring temperature is fixed, implying a fixed apparent atmospheric temperature (Haney 1971), and secondly, although the heat flux is allowed to change, the change actually acts to weaken the oscillation. However, in reality air–sea thermal interactions are present. The present study shows that, even in the presence of such interactions, oscillations persist. This and the role of long Rossby-waves in the generation of interdecadal oscillations have direct geophysical relevance.

Acknowledgements

Wenju Cai is supported by the Australian Department of Environment, Sport and Territories. Peter Chu is supported by the Office of Naval Research High Latitude (HL), Physical Oceanography (PO), and Naval Ocean Modeling and Prediction (NOMP) Programs. Drs S. Rahmstorf and M. Davey provided constructive comments. Harvey Davies provided the plotting routines for the figures. This work was made possible by the pioneering work of the late Michael Cox, and by GFDL for making the MOM code available.

Appendix

Let us simplify the 'flip–flop' model of Pierce *et al.* (1995) to a thermal only system. The salinity is set constant and uniform at S_0 at both layers and the freshwater flux is set zero. The model contains an upper and a lower box with thicknesses of h_1 and h_2, and temperatures of T_1 and T_2, respectively. Temperature T_1 is restored to T_a at the polar boundary, with a coupling strength of K_r equivalent to 45 days. As in the OGCM, surface cooling takes place. This is associated with a heat loss, and, in order to maintain a heat budget, the lost heat is reintroduced into the system as a subsurface heating Q. The heating can be interpreted as a poleward heat transport from the subtropics in a more sophisticated model. In this way Q is the time average of the heat loss. A vertical mixing between the two boxes is allowed and the mixing coefficient is K. The coefficient K is taken to be large when the system is statically unstable, small otherwise, and is always positive.

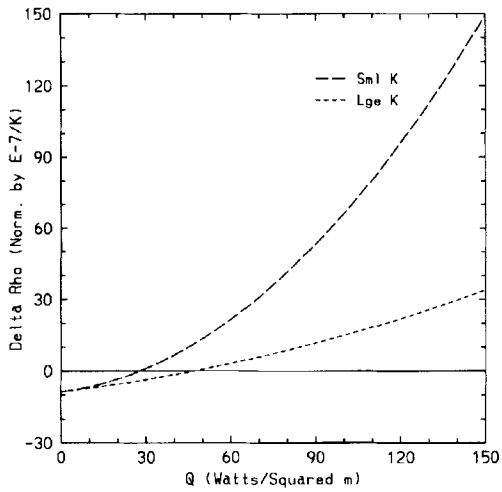

Figure A.1. Dependence of density difference ($\rho_1 - \rho_2$) (kg m^{-3}) upon subsurface heating in a two-layered thermal flip–flop model. When the subsurface heating Q ranges from 26 to 45 W m^{-2}, the flip–flop model is in an oscillatory regime. In this regime, once convection occurs (large K) the water column becomes stable ($\delta\rho < 0$), whereas once convection stops (small K), the water column becomes unstable ($\delta\rho > 0$).

The model equations for temperature are

$$h_1 \frac{\partial T_1}{\partial t} = K_r(T_a - T_1) + K(T_2 - T_1), \tag{A.1}$$

and

$$h_2 \frac{\partial T_2}{\partial t} = Q + K(T_1 - T_2). \tag{A.2}$$

For simplicity, the density equation takes the form used by Zhang *et al.* (1992), i.e.

$$\rho(T, S) = C + AS - B_1 T(1 + B_2 T). \tag{A.4}$$

In this equation, the density (kg m^{-3}) is a linear function of salinity S (parts per thousand) and a nonlinear function of temperature (°C). Zhang *et al.* (1992) showed that when C, A, B_1, and B_2 take values of 1003.0, 0.77, 0.72, and 0.72, respectively, the density approximates well that in the Bryan–Cox model.

In the steady state, the density difference between the boxes is given by

$$\Delta\rho \equiv \rho_1 - \rho_2 = K^{-1}(B_1 Q + 2B_1 B_2 Q T_a + 2B_1 B_2 Q^2/K_r + B_1 B_2 Q^2/K). \tag{A.5}$$

A positive value means that the system is statically unstable and convection occurs; a negative value indicates that the system is statically stable. The system will spontaneously oscillate between convective and non-convective states if the steady state is (1) statically stable ($\Delta\rho < 0$) during convection (with a large K) and (2) statically unstable ($\Delta\rho > 0$) in the absence of convection (with a small K).

Two features emerge from Eq. (A.5). Firstly, given a Q, the only term that is negative so that $\Delta\rho$ may be negative is $2B_1 B_2 Q T_a$ ($T_a < 0$). This term is the product of the surface cooling, nonlinearity, and the subsurface heating. This suggests that for oscillation to be possible, these three processes must all be present. In a linear system $B_2 = 0$, $\Delta\rho$

is always positive, and a non-oscillatory convective state persists. We also see that the nonlinearity acts to stabilize the water column, attempting to produce $\Delta\rho < 0$. Further, the only term that can switch $\Delta\rho$ from positive (convective) to negative (non-convective) as K varies is $B_1 B_2 Q^2/K$. This is again dependent upon the nonlinearity. The physics behind this is simple. Within the water column, buoyancy gain from the subsurface heating provides the source for buoyancy loss by the surface cooling. If the system is linear, the buoyancy gain from the subsurface heating is constant and the system is constantly convective. In the presence of the nonlinearity, the buoyancy gain changes with T_2. During convection, T_2 drops, and the buoyancy gain progressively decreases. There is a point at which the buoyancy gain is too weak to support convection. Once that occurs T_2 rises and the buoyancy gain progressively increases. When the destabilizing buoyancy gain is large enough, convection is initiated again and the cycle repeats itself. Secondly, for a given T_a if Q is small enough, the destabilizing buoyancy gain may not be able to induce convection. In this situation, the system settles to a non-convective steady state. On the other hand, if Q is large enough, the destabilizing buoyancy-flux is not able to be removed by the given cooling strength and a steady convective state results. These features can be seen in Fig. A.1, which shows the dependence of $\Delta\rho$ upon Q given a value of T_a that is the same as in the polar boundary in R45o and a K_r equivalent to 45 days. Other values are $h_1 = 25$ m, $B = 0.072$, $K_1 = 6 \times 10^{-7}$ (when not convecting), and $K_2 = 1 \times 10^4 \times K_1$ (during convection). When the subsurface heating Q ranges from 26 to 45 W m^{-2}, the flip–flop model is in an oscillatory regime.

References

Bryan, F. 1987 Parameter sensitivity of primitive equation ocean general circulation models. *J. Phys. Oceanogr.*, **17,** 970–985

Bryan, K. 1969 A numerical method for the study of the circulation of the world ocean. *J. Comput. Phys.*, **4,** 347–376

1984 Accelerating the convergence to equilibrium of ocean–climate models. *J. Phys. Oceanogr.*, **14,** 666–673

Cai, W. 1994 Circulation driven by observed surface thermohaline fields in a coarse resolution ocean general circulation model. *J. Geophys. Res.*, **99,** 10163–10181

1995 Interdecadal variability driven by mismatch between surface flux forcing and oceanic freshwater/heat transport, *J. Phys. Oceanogr.*, **25,** 2643–2666

1996 Generation of thermal oscillation in an ocean model, *Q. J. R. Meteorol. Soc.*, **122,** 1721–1738

Cai, W. and Godfrey, S. 1995 Surface heat flux parameterizations and the variability of thermohaline circulation. *J. Geophys. Res.*, **100,** 10679–10692

Cai, W., Greatbatch, R. J. and Zhang, S. 1995 Interdecadal variability in an ocean model driven by a small, zonal redistribution of the surface buoyancy flux. *J. Phys. Oceanogr.*, **25,** 1998–2010

Chen, F. and Ghil, M. 1995 Interdecadal variability of the thermohaline circulation and high-latitude surface fluxes. *J. Phys. Oceanogr.*, **25,** 2547–2568

Davey, M. K. 1983 A two-level model of a thermally forced ocean basin. *J. Phys. Oceanogr.*, **13,** 169–190

Delworth, T., Manabe, S. and Stouffer, R. J. 1993 Interdecadal variations of the thermohaline circulation in a coupled ocean–atmosphere model. *J. Climate*, **6,** 1933–2011

Deser, C. and Blackmon, M. L. 1993 Surface climate variations over the North Atlantic Ocean during winter: 1900–1989. *J. Climate*, **6,** 1743–1753

Gill, A. E. 1982 *Atmosphere–Ocean Dynamics* . International Geophysics Series, **30**, Academic Press, San Diego, USA

Gill, A. E. and Bryan, K. 1971 Effects of geometry on the circulation of a three-dimensional southern-hemisphere ocean model. *Deep Sea Res.*, **18,** 685-721

Greatbatch, R. J. and Paterson, K. A. 1996 Interdecadal variability and oceanic thermohaline adjustment. *J. Geophys. Res.*, **101,** 20467–20482

Greatbatch, R. J. and Zhang, S. 1995 An interdecadal oscillation in an idealized ocean basin forced by constant heat flux. *J. Climate*, **8,** 81–91

Griffies, S. M. and Tziperman, E. 1995 A linear thermohaline oscillator driven by stochastic atmospheric forcing. *J. Climate*, **8,** 2440–2453

Haney, L. R. 1971 Surface boundary condition for ocean circulation models. *J. Phys. Oceanogr.*, **1,** 241–248

Holland, W. R. 1973 Baroclinic and topographic influences on the transport in western boundary currents. *Geophys. Fluid Dyn.*, **4,** 187–210

Huang, R. X. 1994 Thermohaline circulation: Energetics and variability in a single hemisphere basin model. *J. Geophys. Res.*, **99,** 12411–12421

Huang, R. X. and Chou, L. 1994 Parameter sensitivity study of the saline circulation. *Climate Dyn.*, **9,** 391–409

Kushnir, Y. 1994 Interdecadal variations in North Atlantic sea surface temperature and associated atmospheric conditions. *J. Climate*, **7,** 141–157

Latif, M. and Barnett, T. P. 1994 Causes of decadal variability over the North Pacific and North America. *Science*, **266,** 634–637

1994 Decadal variability over the North Pacific and North America: dynamics and predictability. *J. Climate*, **9,** 2407–2423

Lenderink, G. and Haarsma, R. J. 1994 Variability and multiple equilibria of the thermohaline circulation, associated with deep water formation. *J. Phys. Oceanogr.*, **24,** 1480–1493

Moore, D. W. and Philander, S. G. H. 1977 'Modelling of the tropical ocean circulation'. Pp. 319–362 in *The Sea*, **6,** Eds. E. D. Goldberg, I. N. McCave, J. J. O'Brien, and J. H. Steele. Wiley-Interscience, California, USA

Pacanowski, R. C., Dixon, K. W. and Rosati, A. 1991 'GFDL Modular Ocean Model, Users Guide Version 1.0'. GFDL Ocean Group Technical Report No. 2, GFDL, Princeton University, Princeton, N. J., USA

Pierce, D. W., Barnett, T. P. and Mikolajewicz, U. 1995 Competing roles of heat and freshwater flux in forcing thermohaline oscillations. *J. Phys. Oceanogr.*, **25,** 2046–2064

Wajsowicz, R. C. and Gill, A. E. 1986 Adjustment of the ocean under boundary forces, Part 1: The role of Kelvin waves. *J. Phys. Oceanogr.*, **16,** 2097–2114

Weaver, A. J. and Sarachik, E. S. 1991a The role of mixed boundary conditions in numerical models of the ocean's climate. *J. Phys. Oceanogr.*, **21,** 1470–1493

1991b Evidence for decadal variability in an ocean general circulation model: an advective mechanism. *Atmosphere–Ocean*, **29,** 197–231

Winton, M. 1996 On the role of horizontal boundaries in parameter sensitivity and decadal-scale variability of coarse-resolution ocean general circulation models. *J. Phys. Oceanogr.*, **26,** 289–304

Winton, M. and Sarachik, E. S. 1993 Thermohaline oscillations induced by strong steady salinity forcing of ocean general circulation models. *J. Phys. Oceanogr.*, **23,** 1389–1410

Wright, D. G. and Stocker, T. F. 1991 A zonally averaged ocean model for the thermohaline circulation. *J. Phys. Oceanogr.*, **21,** 113–1724

Zhang, S., Lin, C. A. and Greatbatch, R. J. 1992 A thermal haline circulation model for ocean climate study. *J. Mar. Res.*, **50,** 99–124